ACCEPTED VERSION

Enrique del Rey Castillo, Michael Griffith, Jason Ingham
Seismic behavior of RC columns flexurally strengthened with FRP sheets and FRP anchors
Composite Structures, 2018; 203:382-395

© 2018 Elsevier Ltd. All rights reserved.

This manuscript version is made available under the CC-BY-NC-ND 4.0 license
http://creativecommons.org/licenses/by-nc-nd/4.0/

Final publication at http://dx.doi.org/10.1016/j.compstruct.2018.07.029

PERMISSIONS

https://www.elsevier.com/about/our-business/policies/sharing

Accepted Manuscript

Authors can share their accepted manuscript:

Immediately

- via their non-commercial personal homepage or blog
- by updating a preprint in arXiv or RePEc with the accepted manuscript
- via their research institute or institutional repository for internal institutional uses or as part of an invitation-only research collaboration work-group
- directly by providing copies to their students or to research collaborators for their personal use
- for private scholarly sharing as part of an invitation-only work group on commercial sites with which Elsevier has an agreement

After the embargo period

- via non-commercial hosting platforms such as their institutional repository
- via commercial sites with which Elsevier has an agreement

In all cases accepted manuscripts should:

- link to the formal publication via its DOI
- bear a CC-BY-NC-ND license – this is easy to do
- if aggregated with other manuscripts, for example in a repository or other site, be shared in alignment with our hosting policy
- not be added to or enhanced in any way to appear more like, or to substitute for, the published journal article

5 November 2020

http://hdl.handle.net/2440/124174

Accepted Manuscript

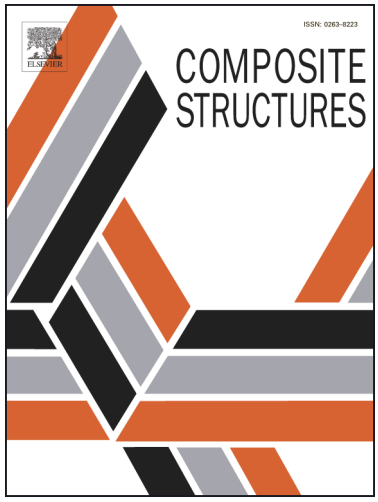

Seismic behavior of RC columns flexurally strengthened with FRP sheets and FRP anchors

Enrique del Rey Castillo, Michael Griffith, Jason Ingham

PII: S0263-8223(18)31071-7
DOI: https://doi.org/10.1016/j.compstruct.2018.07.029
Reference: COST 9946

To appear in: *Composite Structures*

Received Date: 19 March 2018
Revised Date: 5 June 2018
Accepted Date: 4 July 2018

Please cite this article as: del Rey Castillo, E., Griffith, M., Ingham, J., Seismic behavior of RC columns flexurally strengthened with FRP sheets and FRP anchors, *Composite Structures* (2018), doi: https://doi.org/10.1016/j.compstruct.2018.07.029

This is a PDF file of an unedited manuscript that has been accepted for publication. As a service to our customers we are providing this early version of the manuscript. The manuscript will undergo copyediting, typesetting, and review of the resulting proof before it is published in its final form. Please note that during the production process errors may be discovered which could affect the content, and all legal disclaimers that apply to the journal pertain.

ACCEPTED MANUSCRIPT

Seismic behavior of RC columns flexurally strengthened with FRP sheets and FRP anchors

Enrique del Rey Castillo[a], Michael Griffith[b], Jason Ingham[c]

[a]*Lecturer, Dept. of Civil and Environmental Engineering, The University of Auckland, New Zealand. (corresponding author) Email: edel146@aucklanduni.ac.nz*
[b]*Professor, School of Civil, Environmental and Mining Engineering, University of Adelaide, Australia*
[c]*Professor Dept. of Civil and Environmental Engineering, The University of Auckland, New Zealand.*

Abstract

Existing reinforced concrete structures are frequently deemed to be prone to severe damage and/or collapse as a result of the loads that the structure is expected to experience if it were to be subjected to large intensity earthquake shaking. Among the different approaches to elevate the seismic capacity of existing reinforced concrete structures is the use of externally bonded fiber reinforced polymer (FRP) systems, which consist of fiber reinforced polymer sheets soaked in epoxy and bonded onto the concrete surface. However, premature debonding often occurs before the ultimate strength of the carbon fiber sheets is reached, compromising the reliability and/or the efficiency of the intervention. One of the methods to ameliorate premature debonding is the use of fiber reinforced polymer anchors to connect the FRP sheets to the concrete structure, ensuring continuity of the load path.

Six reinforced concrete columns were designed, built and tested to investigate the seismic behavior of the strengthened columns, with five of the columns strengthened with fiber reinforced polymer sheets and anchors. The main objective of the testing program was to experimentally verify that the moment capacity of the FRP strengthened columns was accurately calculated, when accounting for two possible failure modes (failure of the FRP sheets and failure of the FRP anchors). Additional objectives were to investigate the influence of the tension-compression cyclic loading on the capacity of the anchors, assess the influence on column behavior when using fiber reinforced polymer transverse reinforcement, and to investigate the influence on column response when implementing a bond breaking layer.

ACCEPTED MANUSCRIPT

The material properties and column configuration, the design methodology, the observed behavior, and the difference between the calculated and the experimental behavior are thoroughly discussed. A new tri-linear behavior model is proposed and areas of future interest are identified.

Keywords: Seismic strengthening, Reinforced concrete, Square columns, EBR-FRP systems, FRP, FRP anchors

1. Introduction

Reinforced Concrete (RC) has been used as a construction material for more than a century, with the history of concrete design and code development in the USA and in New Zealand having been compiled by MacGregor [1] and Thornton [2] respectively. Existing RC structures are often vulnerable to damage or collapse in the event of a large earthquake and as knowledge on earthquake actions and seismic design improves, new design codes and building standards such as ASCE/SEI 41 [3] appear. The outcome from applying these revised codes and guidelines is often the determination that the evaluated capacity of an existing structure is insufficient to adequately resist earthquake loading, even if the structure was correctly designed following the design code of the era when the structure was designed and built.

Different approaches are available to increase the seismic capacity of existing buildings to meet the criteria established by newly developed codes and standards. The new seismic requirement may be met by increasing the overall structure performance, for example with the incorporation of new shear walls either within or around the existing building. Other approaches can be to enhance the seismic capacity of existing structural members with post-tensioning rods or cables incorporated into the structure, jacketing columns with steel braces, or increasing the cross section of the column with an additional RC confinement, with Rodriguez and Park [4] having presented an in-depth review of various techniques used in different parts of the world. An increasingly used technique to strengthen existing RC structures is the use of Externally Bonded Fiber Reinforced Polymer (EBR-FRP) systems [5, 6]. The main advantages of EBR-FRP systems are the low mass and high tensile capacity characteristic of FRP materials, plus greater durability when properly installed. FRP sheets are the core material in the EBR-FRP system, which are saturated with epoxy resins to form a composite matrix that is adhered to the external surface of the RC structural member.

Different EBR-FRP intervention schemes have been investigated in the past,

ACCEPTED MANUSCRIPT

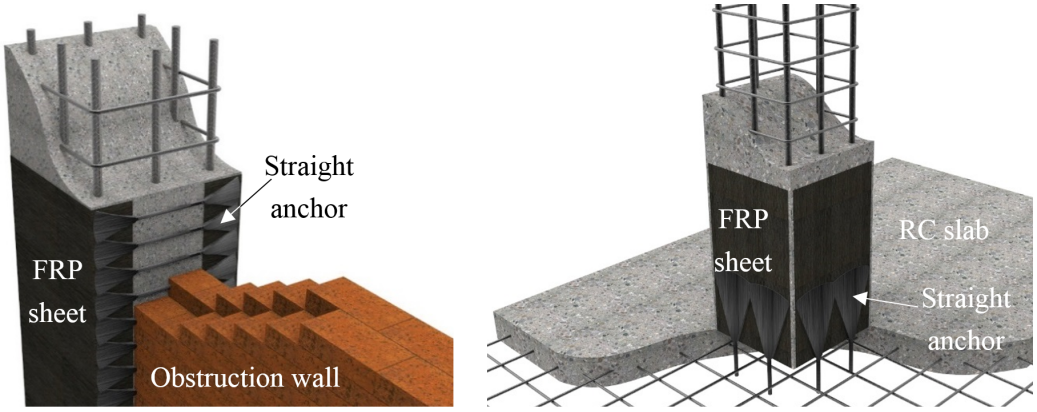

(a) Shear strengthening an RC column (b) Flexural strengthening of an RC column

Fig. 1. Schemes for EBR-FRP strengthening of an RC column

such as shear strengthening and/or repair of beams [7], flexural strengthening of slabs [8] and shear walls [9], and seismic strengthening of columns [10, 11]. Seismic strengthening of columns may address either shear deficient or flexurally deficient columns, with a graphical representation of both schemes being reported in Figure 1. RC columns are more frequently found to be shear deficient and this deficiency is potentially more severe than for flexurally deficient RC columns, because of brittle shear behavior as opposed to the more ductile behavior associated with flexural failure. Nevertheless, flexural ductile failure is still a concern, mainly in bridge piers and at the ground floor of multi-storey buildings. Additionally, more information can be found in the literature regarding the shear strengthening scheme represented in Figure 1a [12, 10] than can be found regarding the flexural strengthening scheme detailed in Figure 1b which has received comparatively little research attention. Finally, after consultation with local engineers it was identified that consulting structural engineers are more confident with the design of the EBR-FRP shear scheme than with the design of the EBR-FRP flexural scheme when FRP anchors are incorporated into the system. The flexural strengthening of columns was therefore identified as the intervention in more urgent need of research attention.

FRP-to-concrete debonding prior to the development of full FRP tensile strength has been highlighted as the main drawback of EBR-FRP systems. Various methods to overcome this problem have been developed and investigated in the past, but FRP anchors have frequently been highlighted as the most appropriate method to address premature FRP-to-concrete debonding [13]. FRP anchors consist of a

ACCEPTED MANUSCRIPT

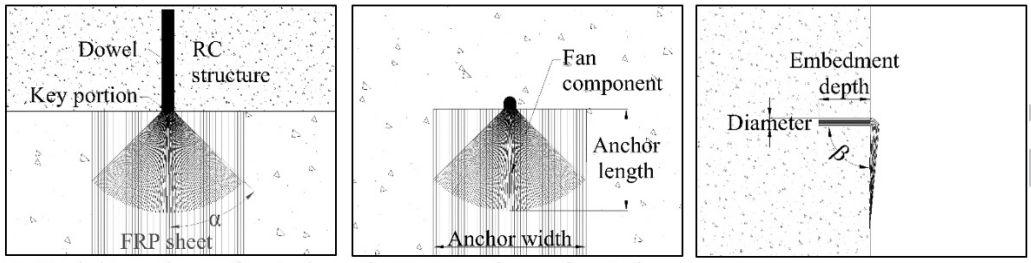

(a) Straight anchor – front view (b) Bent anchor – front view (c) Bent anchor – side view

Fig. 2. Attributes of FRP anchors

bundle of fibers which are soaked in epoxy before being installed, with the main attributes of FRP anchors being represented in Figure 2. One end of the bundle is introduced into a pre-drilled hole in the structure and the other end is splayed out and bonded onto the FRP sheet. FRP anchors feature three main components, with the dowel being introduced into the structure, the fan component being splayed onto the FRP sheet, and the key portion being where the fibers transition from the dowel into the fan. Two main types of FRP anchors are used depending on the angle of insertion β, being straight anchors (Figure 2a) and bent anchors (Figure 2b and c) [14].

Despite the growing use and research attention given to FRP anchors a corresponding design guideline has not yet been produced, which is the main impediment to the implementation of FRP anchors in EBR-FRP systems [13]. Initial attempts to identify and describe failure modes have been undertaken, with a model for the concrete-related failure modes being developed by Kim and Smith [15] and a model for the fan-to-sheet debonding failure mode being developed by Kanitkar [16]. The fiber rupture failure mode of FRP anchors was investigated at an earlier stage of the current research project, which resulted in the development of a number of equations to calculate the ultimate capacity of the anchor when exhibiting the fiber rupture failure mode as a function of the material properties, the fanning angle α and the cross sectional areas. The simplified model reported in Eq 1 for the average value of the ultimate fiber rupture anchor capacity was used.

$$\bar{N}_{fr} = 4.9 E_{FRP} \varepsilon_{FRP} 10^3 A_{dowel}^{0.56} \left(\frac{90 - \alpha}{90}\right) \tag{1}$$

where: $\bar{N}_{fr}$ is the average value of the ultimate fiber rupture capacity of the anchor in kN, E_{FRP} is the elastic modulus of the FRP material in MPa, ε_{FRP} is the

ACCEPTED MANUSCRIPT

strain at rupture of the FRP material in mm/mm, α is the fanning angle in radians, and A_{dowel} is the net cross sectional area of the anchor in mm^2.

The objective of the research program reported herein was to investigate and describe the seismic behavior of RC columns strengthened with FRP sheets and FRP anchors, with the ultimate goal being to verify that the force-displacement and moment-drift response could be accurately calculated when accounting for the different possible failure modes and when implementing the previously developed equation (Eq 1) into the design. Additionally, the effect of tension-compression cycles on the anchors and the influence of the transverse FRP confinement on the column behavior were investigated. Lastly, a novel method consisting of placing a bond breaking layer between the concrete and the FRP sheets was investigated as an attempt to enhance the ductility capacity of the RC column.

2. Experimental program

The material properties and geometric characteristics of the test columns, the process that was followed for the retrofit design, the FRP installation method, and the methodology followed to test the columns is thoroughly discussed in this section.

2.1. Columns properties

A review of RC building typologies in New Zealand was conducted to decide the dimensions and material properties of the RC columns to be designed and built. Several buildings were studied using legacy plans available from the city council archives of Auckland, Wellington and Christchurch, with additional information obtained from previously published studies [17]. Finally, local engineers provided information about an RC structure in Wellington in which the ground floor columns were being strengthened with FRP sheets and FRP anchors following the same scheme as reported in Figure 1. Unfortunately, the structure suffered severe damage during the MW 7.8 Kaikura earthquake in October 2016, before the strengthening scheme could be completed, and the building had to be demolished. The details of column dimensions, steel reinforcement, and FRP materials installed in each column can be seen in Figure 3. The quantity of transverse reinforcement was artificially increased to prevent undesired failure modes such as shear failure or buckling of the longitudinal steel reinforcing bars.

The objective of the column 1 testing was to characterize the behavior of the as-built column and acquire benchmark data for subsequent comparison with the results obtained from testing of the strengthened columns. Column 2, featuring

ACCEPTED MANUSCRIPT

only longitudinal FRP sheets and anchors and no supplementary FRP confinement, was the first attempt to design the EBR-FRP system and to calculate the moment capacity of the FRP strengthened RC column. Additionally, the influence of compression-tension loading cycles on anchor behavior was investigated. Column 3 featured the same FRP configuration as utlised in the retrofit of column 2, but with one layer of FRP transverse confinement being installed over the longitudinal FRP materials to investigate the influence of the FRP confinement on column response. This one layer of FRP confinement was also applied to all the remaining columns (4 to 6). Column 4 was a second attempt to design the FRP anchors, whilst also attempting to elevate the flexural strength of column 4 when compared with the flexural strengths of columns 2 and 3. To achieve an elevated moment capacity for column 4 the number and size of anchors was increased from three anchors in columns 2 and 3 that each had a net cross sectional area of 84 mm^2, to four anchors in column 4 that each had a net cross sectional area of 112 mm^2. The targeted failure mode of the retrofit design for columns 2, 3 and 4 was rupture of the FRP anchors at the column-foundation joint.

The retrofit schemes of columns 5 and 6 were designed to shift the location of fiber rupture from the FRP anchors at the column-foundation interface, to instead occur in the FRP sheets at the position where the FRP anchors terminated (approximately 280 mm from the column-foundation interface). To achieve this shift in failure position for columns 5 and 6 the number and size of anchors was increased to 6 anchors that each had a net cross sectional area of 168mm^2, and the number of longitudinal sheets was reduced from three sheets to two sheets. Additionally, column 6 featured a bond breaking layer over the bottom half metre of the column, close to the column-foundation interface, with the objectives of the bond breaking layer being to shift upwards the height at which FRP-to-concrete debonding commenced and to enable the influence of this debonding shift on the lateral displacement and ductility capacity of the column to be observed. The rationale and design process for each of the deployed EBR-FRP systems are discussed below.

2.2. Material properties

Two concrete mixes were used, with one mix having a target compressive strength of 50 MPa for the foundation slab and the second mix having a target compressive strength of 40 MPa for the six columns. The two concrete mixes were delivered with a 15 day interval, during which time the transverse reinforcement and the formwork for the columns were installed. The average compressive and tensile strength of each concrete mix reported in Table1 was determined using

ACCEPTED MANUSCRIPT

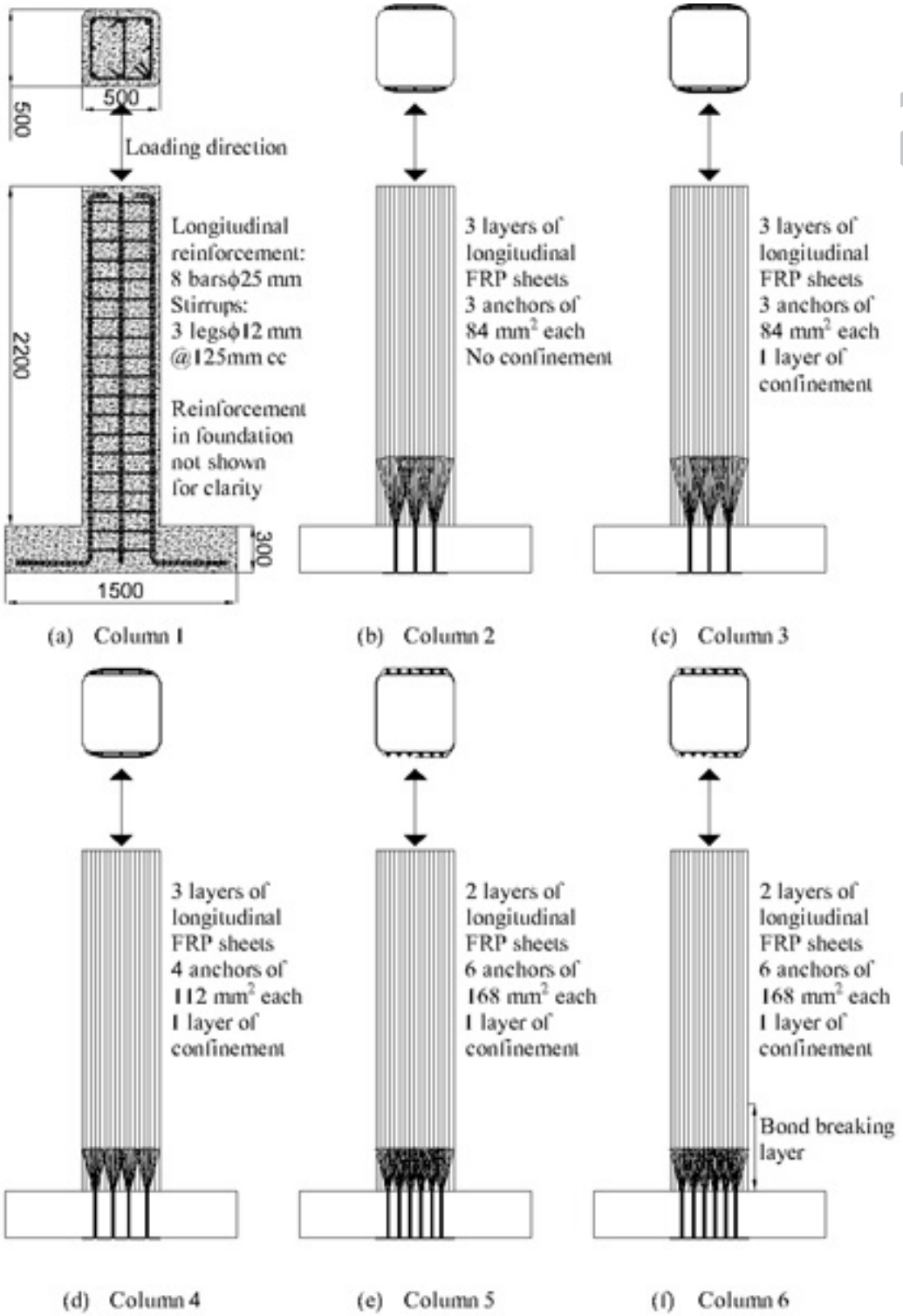

Fig. 3. Columns dimensions, steel reinforcement and EBR-FRP details

ACCEPTED MANUSCRIPT

Table 1. Concrete mechanical properties

	Column age (days)				Foundation age (days)			
	7	23	28	333	7	28	43	353
Compressive strength (MPa)	34.3	36.6	38.9	44.3	43.4	49.9	52.5	56.2
Tensile strength (MPa)	2.4	3.3	3.5	4.0	4.5	5.2	5.4	5.8

Table 2. FRP material net-fiber properties

	Net fiber thickness (mm)	Tensile Modulus E (GPa)		Tensile strength σ (MPa)		Ultimate strain ε (%)	
		$\bar{x}$	Design	$\bar{x}$	Design	$\bar{x}$	Design
FRP fabric	0.331	75.7	68.1	968	833	1.3	1.1
FRP Anchor†	28 mm^2	-	230	-	2100	-	1.6
FRP Anchor‡	28 mm^2	-	253	-	2479	-	1.0
† Manufacturer-specified properties [19, 20], ‡ Experimentally-obtained properties [21]							

concrete cylinders in accordance with NZS 3112-2 [18], in close agreement with the target values.

One type of FRP fabric and one type of FRP bundle were used to strengthen the columns, with the net-fiber material properties for the FRP products and for the epoxy resin used in this research project being reported in Table2 and Table3 respectively. The manufacturer-specified properties are the material properties specified in the manufacturer's datasheets, while the experimentally-obtained properties were evaluated by Sika Spain following an internal experimental program. The ultimate strain was similar for both materials, being 1.1% and 1.0%.

Table 3. Manufacturer-specified resin material properties (SIKA 2013a)

	Tensile modulus (GPa)	Tensile strength (MPa)	Ultimate strain (%)
7 days at 23C	3.5	45.0	1.5
72 hours at 60C	3.2	72.5	4.8

ACCEPTED MANUSCRIPT

Table 4. Assumed concrete properties for each column

Column number	Age (days)	$f_c^{'}$ (MPa)	$f_t^{'}$ (MPa)	$f_{cc}^{'}$ (MPa)	ε_{cc} (%)	$f_{tc}^{'}$ (MPa)
2	51	42.4	3.6	46.8	0.716	4.0
3	135	44.3	3.7	48.7	0.724	4.1
4	213	46.0	3.9	50.4	0.731	4.3
5	261	47.0	4.0	51.4	0.734	4.4
6	282	47.5	4.0	51.9	0.736	4.4

Where:
$f_c^{'}$ is the compressive strength experimentally obtained from cylinders in MPa,
$f_t^{'}$ is the tensile strength experimentally obtained from cylinders in MPa,
$f_{cc}^{'}$ is the confined compressive strength calculated from ACI 440 in MPa,
ε_{cc} is the confined concrete strain calculated from ACI 440 in %, and
$f_{tc}^{'}$ is the confined tensile strength linearly calculated from in MPa.

2.3. Design process

Response 2000 is a reinforced concrete sectional analysis program developed at the University of Toronto, which was used to design the column cross-section and calculate the behavior of each of the six columns. The concrete compressive and tensile strength and the concrete compressive strain at peak strength were obtained from cylinder testing conducted in accordance with NZS 3112-2 [18] at four different ages, which were not coincident with the time of column testing. The concrete properties used to model the columns in Response 2000 were linearly interpolated based on the age of each column and used as input data to manually calculate the confined concrete strength and strain calculation defined in ACI 440 [22] for the strengthened columns. The concrete compressive strength experimentally obtained from the cylinder tests and the FRP-confined concrete strength and strain at peak strength calculated from ACI 440 are summarized in Table 4. The FRP-confined concrete tensile strength was linearly interpolated based on the cylinder tensile strength data reported in Table 1 and the FRP-confined compressive strength. The concrete material properties were modeled in Response2000 using the Popovics base curve model [23], the Vecchio-Collins compression softening model [24], and the Bentz tension stiffening model [25].

The steel reinforcement was modeled in Response 2000 as a bilinear elasto-perfectly plastic material using the experimentally obtained results. The FRP was modeled assuming brittle and fully linear-elastic behavior and the material

ACCEPTED MANUSCRIPT

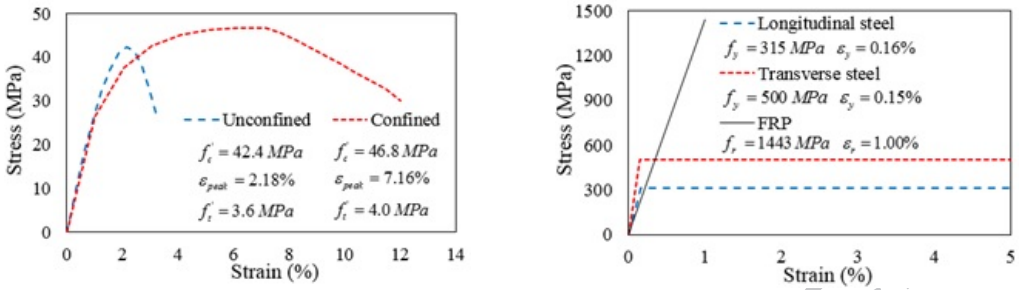

(a) Concrete model for column 2 (b) Reinforcement model

Fig. 4. Schematic representation of constitutive material models

properties from Table 2, with a schematic representation of the constitutive material models being reported in Figure 4.

The as-built moment capacity of column 1 was calculated to be 367 kNm using Response 2000. For columns 2 and 3 a strengthening target of 30% improvement in moment capacity (to 477 kNm) was adopted, while a 50% moment capacity improvement (to 550 kNm) was adopted for column 4 and a 75% moment capacity improvement (to 642 kNm) was adopted for columns 5 and 6. Sectional analysis was used to establish the ultimate tensile force that the longitudinal FRP materials had to resist for these elevated column moment capacities, resulting in minimum tensile forces in the FRP materials of 330 kN for columns 2 and 3, 500 kN for column 4, and 600 kN for columns 5 and 6.

Three anchors were utilized for columns 2 and 3, which resulted in each anchor having to sustain 110 kN. Using Eq 1 and the material properties in Table 2, each anchor required a minimum net cross sectional area of 73.9 mm^2, but because multi-bundle anchors are made up of two or more bundles combined together, the actual net cross sectional area was larger than the minimum net cross sectional area. Three bundles per anchor were used for columns 2 and 3, which resulted in an actual net cross sectional area of 84 mm^2. Similarly, four anchors with four bundles in each anchor were used in column 4, giving an actual net cross sectional area of 112 mm^2. The number of longitudinal FRP sheets used in columns 2, 3 and 4 was increased to ensure that the sheets would not break. Conversely, the longitudinal FRP sheet configuration in columns 5 and 6 was designed for the longitudinal FRP sheets to fail at a load of 600 kN, while the anchors were design to be stronger than the longitudinal FRP sheets. The resulting anchor design in columns 5 and 6 featured six anchors each composed of six bundles. The absolute target moment

ACCEPTED MANUSCRIPT

Table 5. FRP design details

Column number	Absolute target moment capacity (%/kNm)	Tension force in the FRP materials (kN)	Total minimum and actual net cross sectional area of anchors (mm^2)	Number of anchors and number of bundles per anchor	Total minimum and actual net cross sectional area of sheets (mm^2)	# of sheets
2-3	130/477	330	221.7 / 252†	3 anchors of 3 bundles	496.5	3
4	150/550	500	375.6 / 448†	4 anchors of 4 bundles	496.5	3
5-6	175/642	600	1008	6 anchors of 6 bundles	197.4/331†	2

†FRP material design to fail. The properties of the FRP materials are provided in Table 2

capacity expressed as both a percentage of the moment capacity of the as-built column and in terms of the required flexural strength, the corresponding minimum tension force that the FRP materials needed to sustain, the minimum and actual cross sectional areas, and the configuration of FRP anchors and FRP sheets are reported in Table 5.

The peak moment capacity of the columns was calculated based on the FRP rupture strain, but a debonding moment was theorized to occur when the FRP-to-concrete debonding was initiated at the bottom end of the FRP sheet, next to the column-foundation joint. The end sheet debonding strain (also known as end plate debonding) was calculated using Section 4.1.2 of CNR DT 200 [26], with the resulting debonding strain being equal to 0.21% for columns 2, 3 and 4 and equal to 0.25% for columns 5 and 6, with the difference attributable to the number of longitudinal sheets used in each column.

The FRP configurations reported in Table 5 were designed to obtain a fiber rupture failure mode either in the anchors (columns 2 to 4) or in the sheets (columns 5 and 6). The fan-to-sheet debonding failure mode was prevented by maintaining a sufficiently large fan area, assuming two fan areas because the fan components were sandwiched between two longitudinal FRP sheets as explained below. To prevent concrete-related failure modes the anchor dowels were passed all the way through the foundation and splayed out onto the underneath surface of the foundation. While passing the anchors all the way through the foundation is an easy solution

ACCEPTED MANUSCRIPT

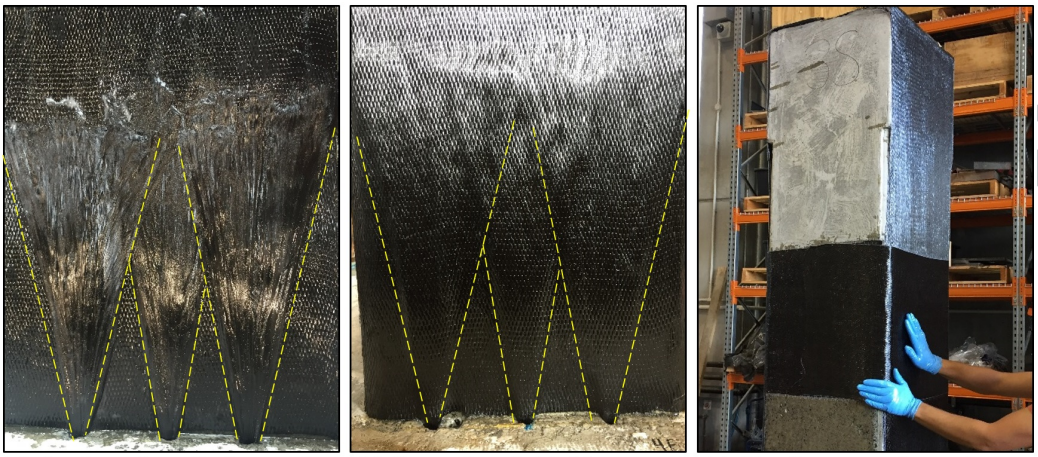

(a) Anchors installed onto first layer of longitudinal sheets

(b) Second and third layers of longitudinal sheets installed on top of the anchors

(c) Confinement sheets being installed on top of the longitudinal sheets

Fig. 5. FRP material installation details

when drilling through inter-storey floors in a real installation, drilling underneath the foundation is not practical when anchoring through the foundation slab. In these cases a full study of the concrete related failure modes must be undertaken, which was outside the scope of the present study.

2.4. FRP material installation process

After the concrete had cured the column surface was ground to expose the aggregates and the concrete pores and to remove any remaining dust particle, thus leading to an improved FRP-to-concrete bond. The holes for the anchors were drilled using a fiber-to-total volume ratio of 0.5, with the cured cross sectional area of the dowel being twice the net cross sectional area. Once the columns were ready the first FRP sheet was installed onto the concrete surface, followed by the FRP anchors and the rest of the FRP sheets, and finished with the transverse confinement, with photographs of the FRP installation process presented in Figure 5. Column 6 featured a plastic sheet to act as a bond breaking layer around the concrete over the bottom half meter of the column.

2.5. Testing set-up and loading protocols

The testing set-up can be seen in Figure 6, with eight post-tensioned rods passing through the foundation slab and securing the foundation to the strong floor. Two additional rods were used to post-tension the foundation slab horizontally,

ACCEPTED MANUSCRIPT

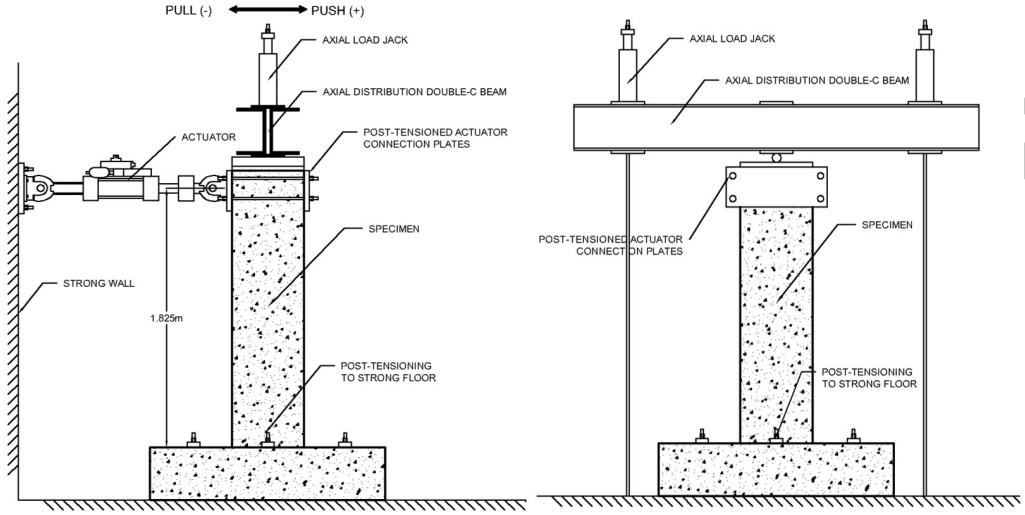

(a) Side view (b) Front view

Fig. 6. Testing set-up

increasing the strength and allowing the foundation slab to be reduced in size. Lateral load was applied using a hydraulic actuator that incorporated a Linear Variable Differential Transformer (LVDT) and a load cell to measure the lateral displacement and applied load. A double C-channel beam was positioned on top of the column in the direction perpendicular to the applied lateral load and a vertically-oriented post-tensioning rod was installed at each end of the C-channel beam to apply axial load to the top of the column, as shown in Figure 6. This axial load was applied to each post-tensioning rod using a hydraulic jack and was measured with a load cell. The post-tensioning rods and hydraulic jacks can be seen in Figure 6, but the load cells and hydraulic pumps have not been represented for clarity. The displacements and strains of the FRP material were measured using the Digital Image Correlation (DIC) technique.

The loading protocol described in ACI 374 [27] was used for columns 1 and 2. This protocol was designed for RC columns and consists of two lateral drift increments up to the yield point, with at least two cycles for each increment. After the yield point the lateral drift increments corresponding to the yield lateral drift are applied as represented in Figure 7a. The inelastic increment of column 2 was reduced to better capture FRP rupture, resulting in a large number of cycles. A different loading protocol was used for the remaining columns, based on similar studies such as [28, 29] and the behavior observed in column 2. This new loading

ACCEPTED MANUSCRIPT

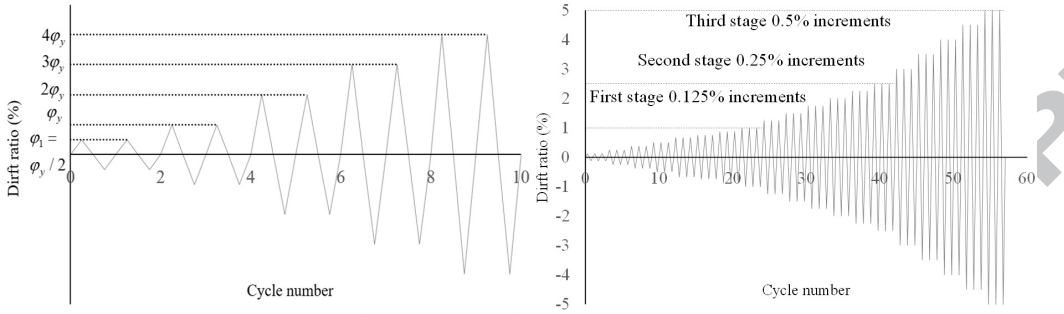

(a) Loading protocol according to ACI 374 (b) Loading protocol for columns 3 to 6

Fig. 7. Loading protocols used in the project

protocol consisted of a 0.125% incremental lateral drift up to 1%, followed by a 0.25% increment in lateral drift from 1% to 2.5% and a 0.5% increment in lateral drift from 2.5% to 5%, as per Figure 7b. Three cycles instead of two were applied at each lateral drift level, due to the large damage observed in column 2 when the second and third cycles were applied. The lateral loading rate was maintained below 1 mm/sec.

3. Experimental results

The applied lateral force, the lateral displacement, the moments and drifts calculated from these loads and displacements, photographic records of the observed failure, and examples of the strain fields obtained using DIC are reported in this section. In Figure 8 the force-displacement and the corresponding moment-drift hysteresis curves are plotted in red for each column. The backbone curves were extracted from the hysteresis curves and are plotted as black dash lines. During the testing of column 1 an equipment failure triggered the actuator to rapidly push the column to the maximum stroke when inelastic response was expected to commence, and the data up to that failure position is plotted in Figure 8 in red. The backbone curve of column 1 was obtained using Response 2000[30] and validated with the hysteresis curves from column 2 after the FRP anchors failed. This post-failure behavior, represented in purple in Figure 8, corresponded to the predicted as-built behavior. The back bone curve of column 1 has been plotted in columns 2 to 6 as a cyan dash line to compare the strengthened behavior of each column with the as-built behavior. Column 2 was only tested up to a drift ratio of 3%, at which point the test was stopped for safety reasons.

ACCEPTED MANUSCRIPT

The behavior of all strengthened columns was comparable, with a first elastic state followed by an inelastic state that concluded at the peak load. The lateral load then decreased as the lateral displacement increased until all the longitudinal FRP materials had ruptured and response aligned with the as-built behavior. The behavior of each column and the observed failure modes are further explained in detail in the following section. The lateral strength increased from columns 2 and 3 to column 4 and further to columns 5 and 6, in accordance with the intended design. The lateral displacement at the end of the elastic state was comparable between the different columns but the drift at peak moment was different for the columns, depending on the amount of FRP materials installed on the column. The drift at peak moment for column 6 was significantly larger than the drift at peak moment of the other columns, even when compared with column 5 that featured the identical strengthening scheme but without the bond breaking layer. This observation indicates that a bond breaking layer that increases the height up the column where FRP-to-concrete debonding initiates is an effective method to control the column ductility capacity. Quantification of the moments and drifts at each behavior stage are considered below, together with further discussion.

A further observation that can be inferred from the graphs in Figure 8 is the high asymmetric response of the columns, especially when drifts were large and the FRP materials were progressively failing. This asymmetric response is further discussed later.

3.1. Behavior and failure mode

The lateral applied force-displacement and corresponding moment-drift backbone curves are plotted in Figure 9. Column 1 did not exhibit the behavior typically expected for RC columns, with a significant post-peak strength reduction as the concrete cover spalled, the longitudinal bars buckled, and the transverse stirrups ruptured. Instead, this behavior was prevented by the additional transverse steel reinforcement provided to the column, which resulted in the strength continuing to increase as the longitudinal reinforcement yielded. Loss of gravity load carrying capacity was not observed in any of the six column tests. As can be seen in Figure 9, the commonly assumed idealized bilinear behavior cannot be directly applied in FRP-strengthened RC columns because these bilinear curves do not capture the actual behavior of the columns, especially in the peak moment region. FRP strengthened RC columns feature 3 different behavior stages, being (1) an elastic behavior, (2) inelastic hardening, and (3) inelastic degradation, followed by return to the response traced by the as-built behavior.

ACCEPTED MANUSCRIPT

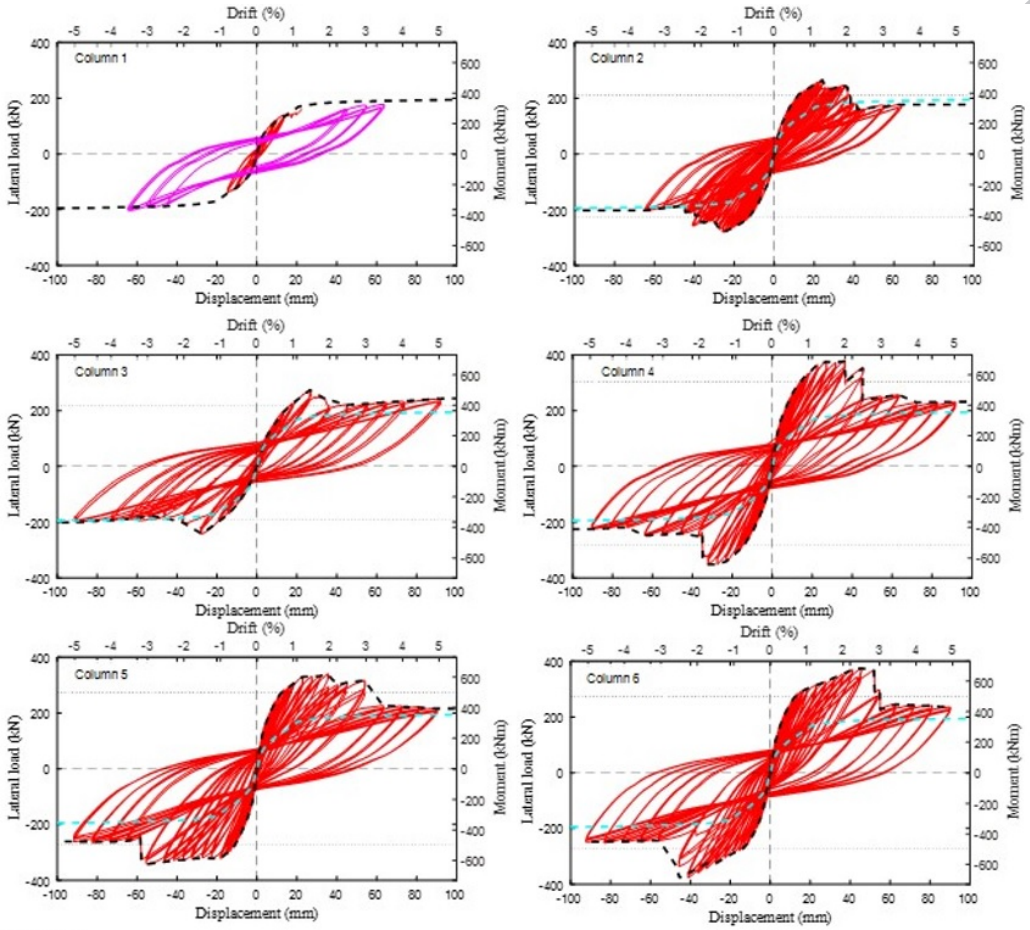

Where:

Red continuous line represents hysteresis loops,
Black dash line represents backbone curve,
Black dotted line represents 80\% of peak load,
Purple line in column 1 plot represents post-FRP rupture behavior of column 2, and
Cyan dash line represents as-built behavior in columns 2 to 6

Fig. 8. Force-displacement hysteresis loops for each column

ACCEPTED MANUSCRIPT

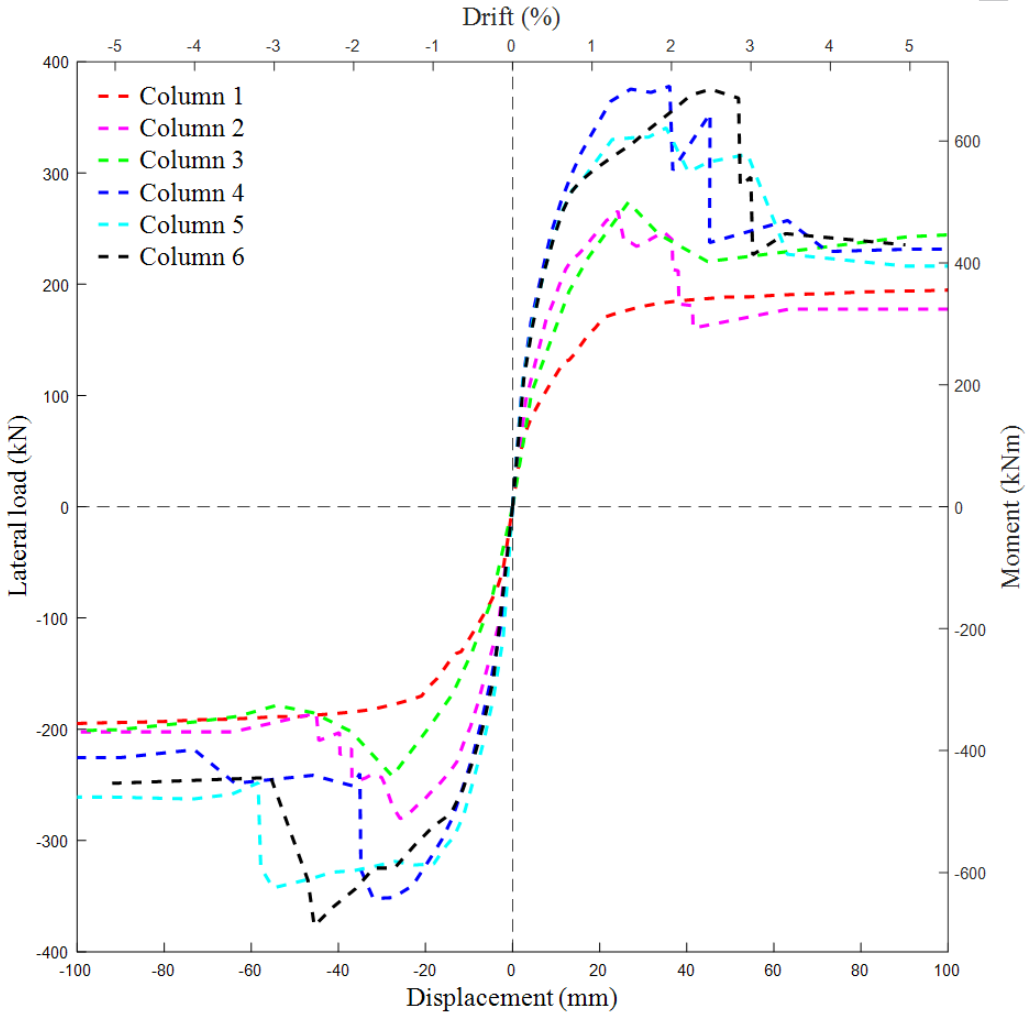

Fig. 9. Backbone curves for each column

ACCEPTED MANUSCRIPT

3.2. First stage - Elastic behavior

The first stage of force-displacement response spanned from the beginning of the test to the development of the moment at which first FRP-to-concrete debonding occurred, defined by the debonding moment. The debonding moment, which was equal to approximately 80% of the peak moment, occurred when the strain in the FRP reached the end-plate debonding strain as calculated with Section 4.1.2 of CNR DT 200 [26]. Arguably, two other stages exist, being defined by the concrete crack strain and the steel yield strain. However, the cracking moment was found to be insignificant and the FRP confinement prevented the cracks from being properly detected and measured. The FRP debonding strain and the steel yield strain occurred almost simultaneously because the debond strain and the yield strain are similar (0.16% and 0.21%) and because of the small distance within the section between the steel rebar and the FRP sheet.

This first stage of force-displacement response was characterized by thin hysteresis loops, with no significant degradation being observed in the second and third cycle loops or by visual inspection, and no residual displacement being recorded. A single thin crack appeared at the column-foundation joint but no damage was observed in the concrete or in the FRP materials and no sounds of cracking or debonding were heard. The hysteresis loops corresponding to the first stage of column 6 are reported in Figure 10.

The longitudinal strain fields from -2% strain (compression) to +2% strain (tension) from two columns are reported for the three stages described in this section. On the left side DIC results obtained from column 6 are reported while on the right side the DIC reported results were obtained from column 2. As a reminder, column 6 failed by rupture of the longitudinal sheets while column 2 failed by rupture of the anchors. The DIC results reported in Figure 11 were smooth and below the ultimate strain of the FRP, although high strain ratios were starting to concentrate at areas where damage eventually occurred.

3.3. Second stage - Inelastic hardening.

The second stage of force-displacement response spanned from the moment when the debonding strain was reached in the FRP material (which indicated the beginning of the FRP-to-concrete debonding process) to the moment when the rupture strain was reached in the FRP material after the FRP-to-concrete debonding process had concluded. The end of this stage indicated that the peak moment had been reached and that the FRP rupture process had initiated, marking the beginning of the third stage of force-displacement response. The blue hysteresis loops in Figure 12 represent the behavior of the first stage while the black loops represent

ACCEPTED MANUSCRIPT

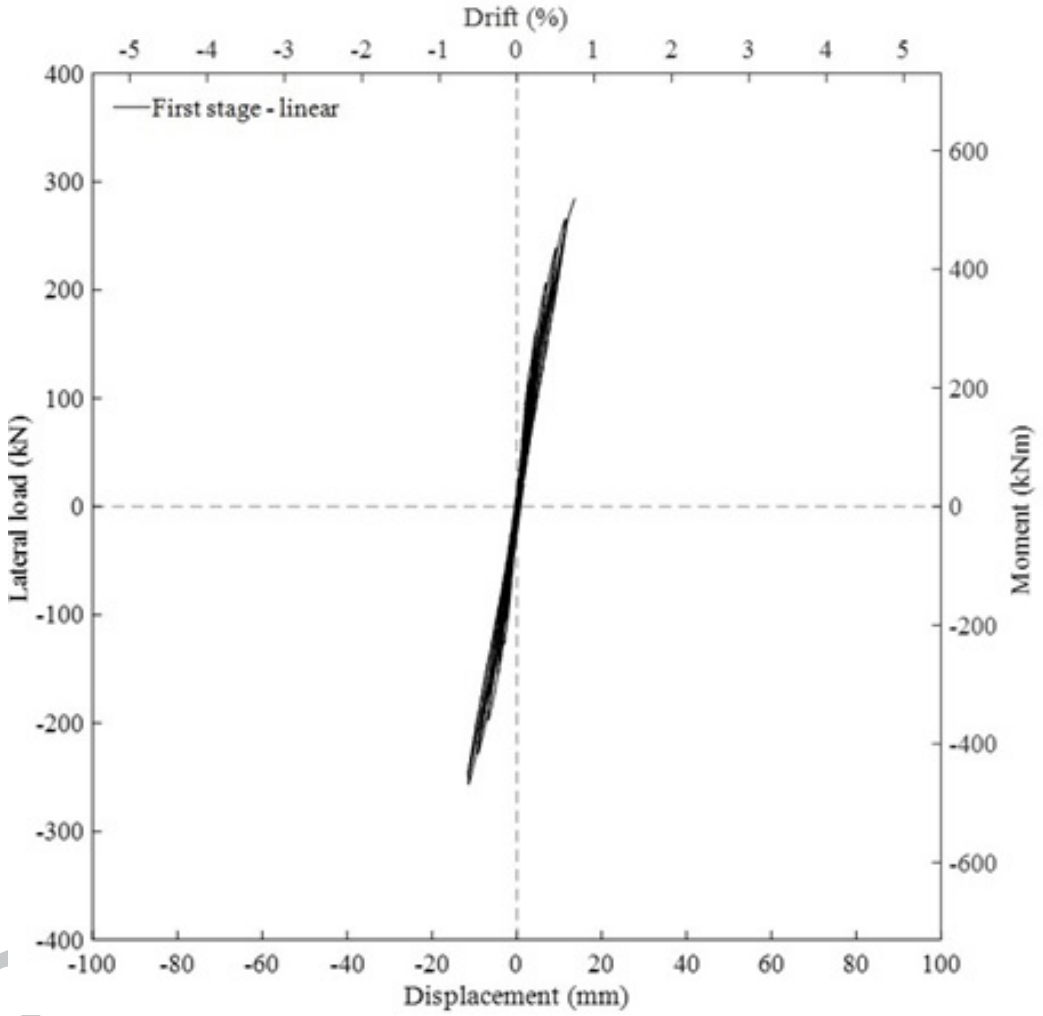

Fig. 10. Hysteresis loops in the first stage of testing – Column 6

ACCEPTED MANUSCRIPT

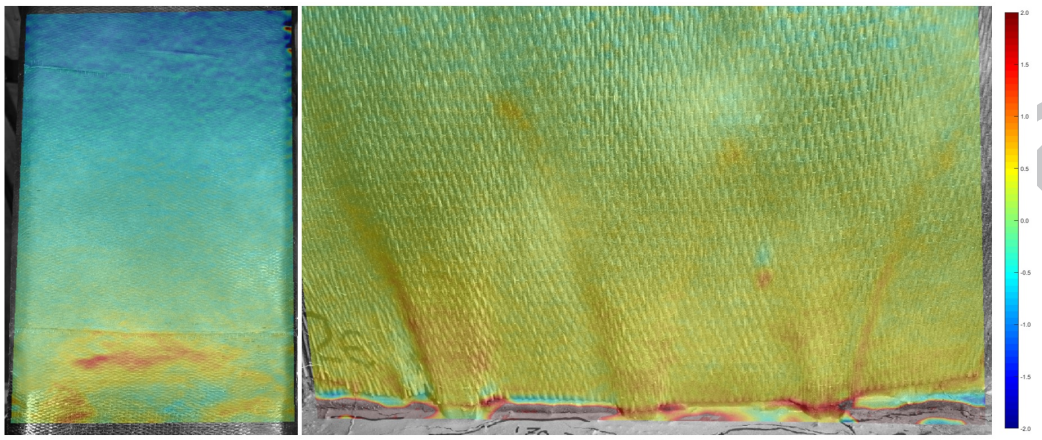

(a) Results on sheets – Column 6 cycle to ±1\% drift

(b) Results on anchors – Column 2 cycle to ±1\%drift

Fig. 11. Longitudinal strain DIC results from the first stage of testing

the behavior of the second stage. The loops broadened, with the second and the third cycle featuring a significant drop in applied lateral load for the same lateral drift, and the residual displacement increased. The drop in lateral applied load and the increase in residual displacement was caused by FRP-to-concrete debonding, which resulted in damage to the top layer of concrete. The loops remained regular, homogeneous and relatively symmetrical at this stage, especially when the behavior of column 6 is compared to the behavior of the other columns. The progress of the FRP-to-concrete debonding process in column 6, which was detected with cracking sounds and the help of the coin-tapping technique, occurred when the FRP materials were subjected to tension. Conversely, the FRP-to-concrete debonding process in columns 2 to 5 started when the FRP materials were subjected to compression forces because the FRP material could not accommodate the shape of the deformed column. The bond breaking layer at the bottom of the column prevented premature debonding in the compression cycle by accommodating the FRP buckling in the debonded area, resulting in a more regular and homogeneous FRP-to-concrete debonding process.

The damage suggested by the hysteresis loops can be observed in Figure 13 and in the DIC results shown in Figure 14. The rupture of the longitudinal FRP sheets in column 5 can be seen in Figure 13a, while the first fiber rupture observed in the anchors installed in column 2 is reported in Figure 13b. Similarly, using DIC the first sheet failure in column 5 and the first anchor failure in column 2

ACCEPTED MANUSCRIPT

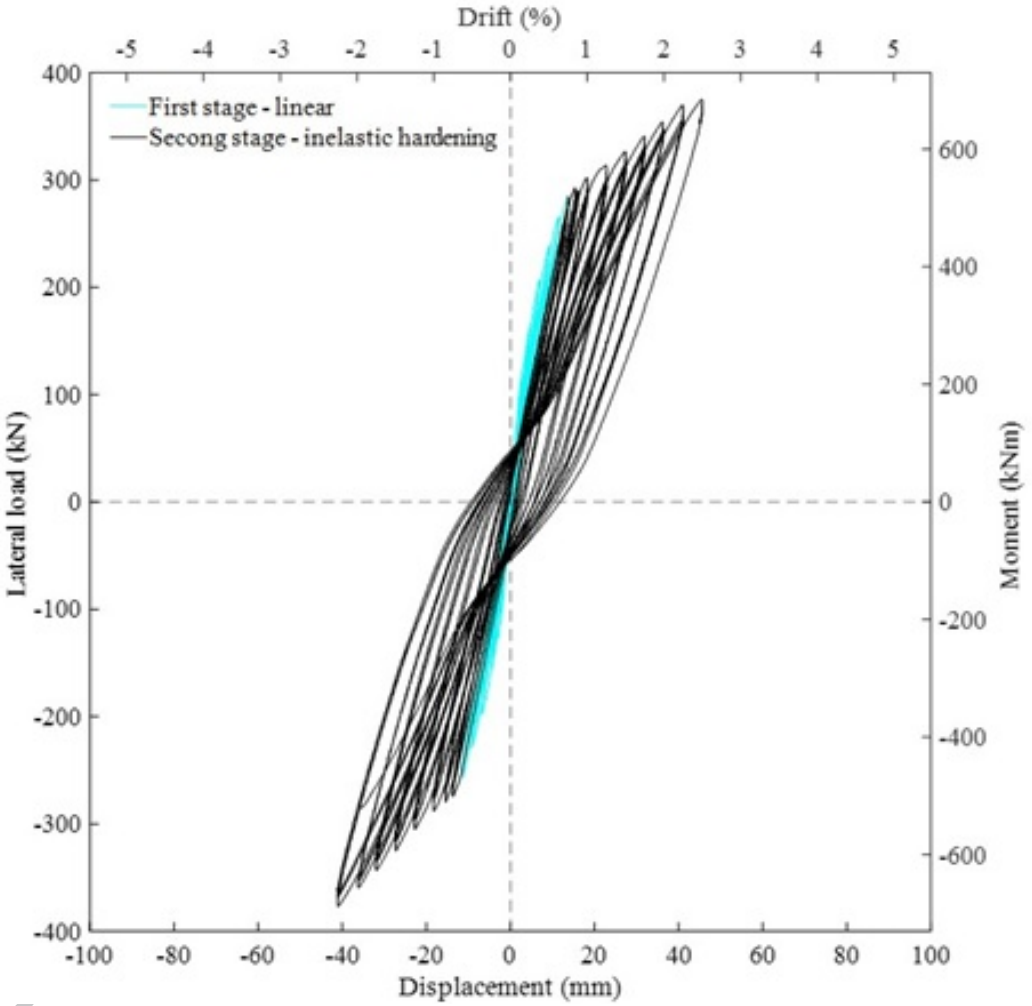

Fig. 12. Hysteresis loops in the second stage of testing – Column 6

ACCEPTED MANUSCRIPT

(a) First longitudinal FRP sheet damage - Column 5

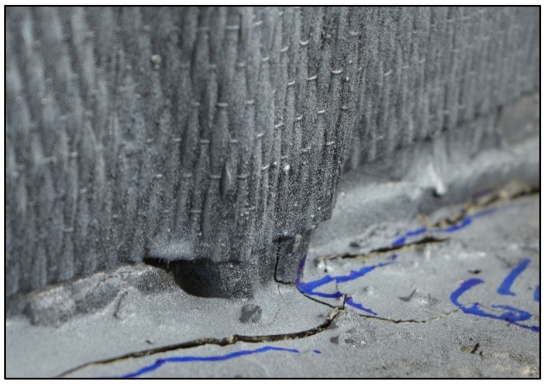

(b) Concrete crack at the bottom of the column and first FRP crack in the anchor – Column 2

Fig. 13. Damage observed in the FRP materials

were detected, with the observed DIC results being reported in Figure 14a and Figure 14b respectively.

3.4. Third stage – Inelastic degradation.

The hysteresis loops corresponding to the third stage of force-displacement response are reported in black in Figure 15, with the loops from the first and the second stages being represented in cyan and green respectively. The as-built behavior, observed after the third stage was concluded, is represented with red loops. The loops were broader in the third stage than in the previous two stages, indicating that the rupture of the fibers had commenced, which was also visually observed in the FRP sheets and anchors. This stage spanned the duration of the FRP rupture, with the duration and shape of the hysteresis loops from this stage varying from one column to another and even from the push to the pull directions within the same column. This asymmetric behavior within the pull and push direction of the same column was especially significant in column 5, which featured a long duration of the third stage in the push direction but a short duration in the pull direction, meaning that the behavior was more brittle in the pull direction than in the push direction. By contrast, column 6 behaved similarly in both the push and the pull direction with sudden drops in load being observed as fibers ruptured, which are represented by red circles in Figure 15. The bond breaking layer probably contributed to have a more regular behavior in the third stage. The behavior of the columns during this third stage may be sensitive to the loading protocol applied because the fibers progressively ruptured as the displacement was

ACCEPTED MANUSCRIPT

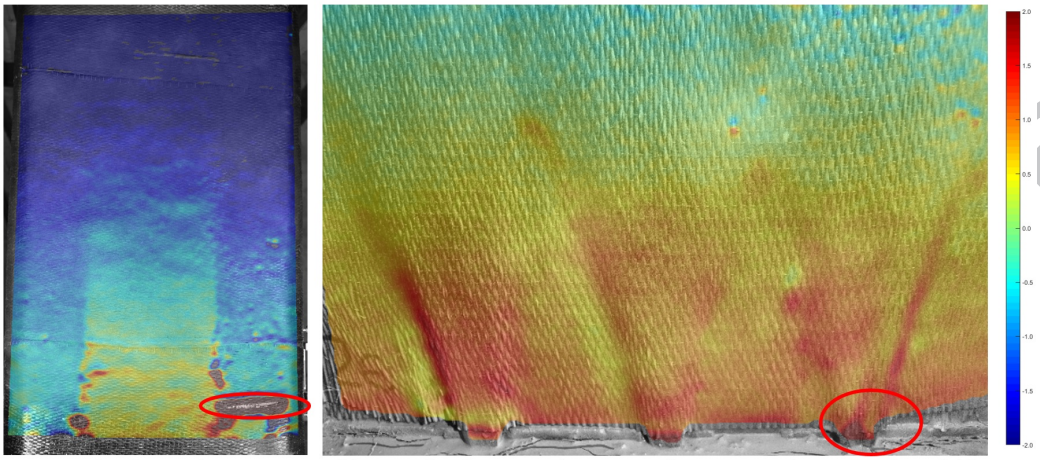

Results from sheets – Column 5 cycle to ±2.5\% drift

(b) Results from anchors – Column 2 cycle to ±2.5\% drift

Fig. 14. Longitudinal strain DIC results from the second stage of testing

increased, and the applied lateral load dropped. Degradation in the second and third cycles was more significant than in the previous two stages, representing the progressive rupture of the FRP fibers as detected with DIC in Figure 16. The rupture of the FRP fibers could be heard with loud explosive noises, and visually detected on the FRP materials as reported in Figure 17. When all the longitudinal fibers were broken at the end of the third stage the as-built behavior was resumed.

3.5. Proposed behavior characterization

The behavior observed during testing and reported in the previous section corroborated the hypothesis that two critical moments exist when designing FRP strengthened RC columns, (1) an FRP-to-concrete debond moment and (2) an FRP rupture moment. The experimental tri-linear behavior is reported in Figure 18, with the initial line corresponding to the elastic stage and the secondary line corresponding to the inelastic hardening stage. The third stage can be simplified as an instantaneous loss in moment capacity for a constant drift ratio (the vertical lines in Figure 18). The main reason for this simplification is that the third stage differed significantly from column to column and was potentially influenced by the loading protocol. After the loss in moment capacity the behavior can be assumed to resume to that of the as-built column.

The debonding drift was similar for all columns because the debonding strain was primarily dependent on the concrete properties, which did not differ signifi-

ACCEPTED MANUSCRIPT

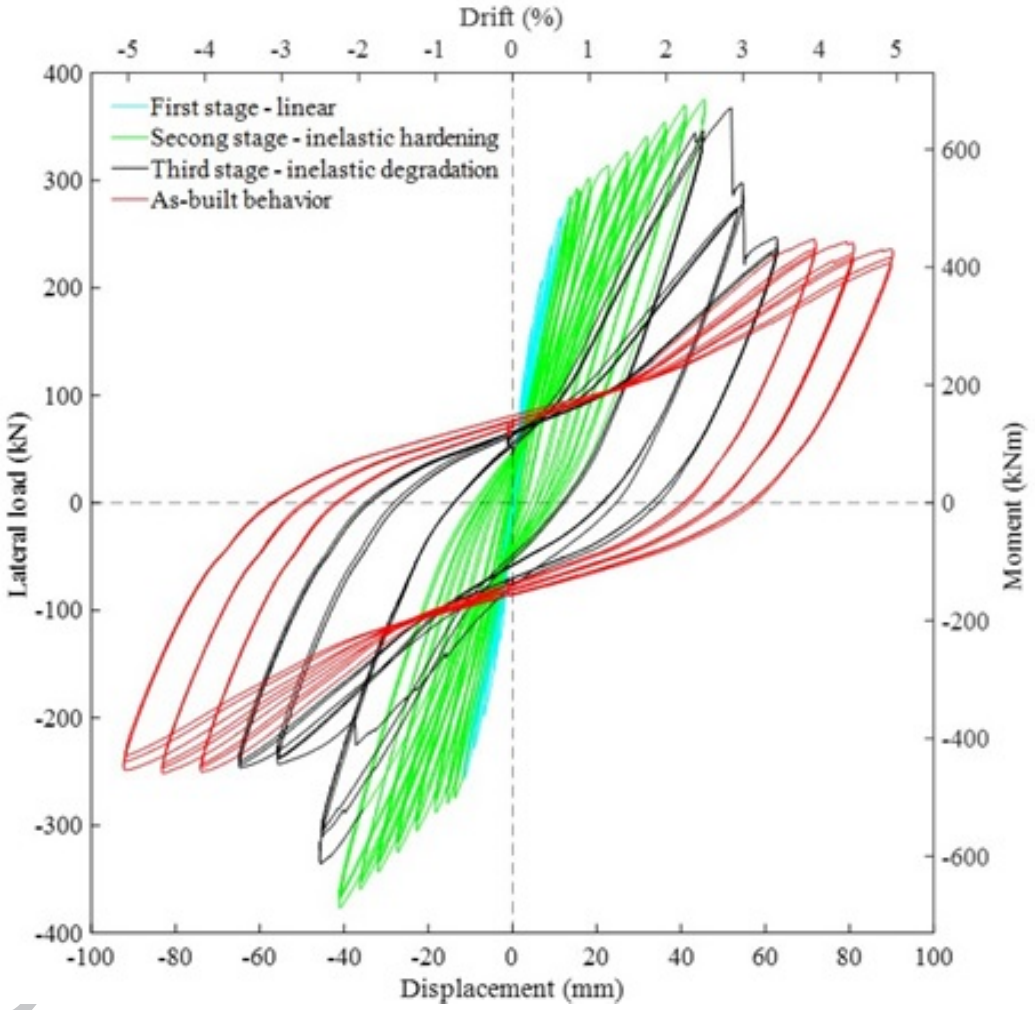

Fig. 15. Hysteresis loops in the third stage of testing – Column 6

ACCEPTED MANUSCRIPT

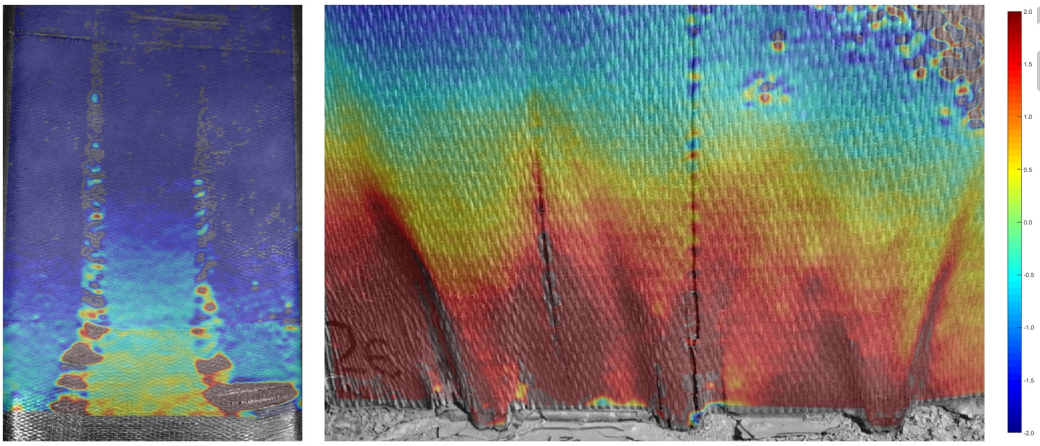

(a) Results from sheets – Column 5 cycle to ±5\% drift

(b) Results from anchors – Column 2 cycle to ±5\% drift

Fig. 16. DIC results from the third stage of testing

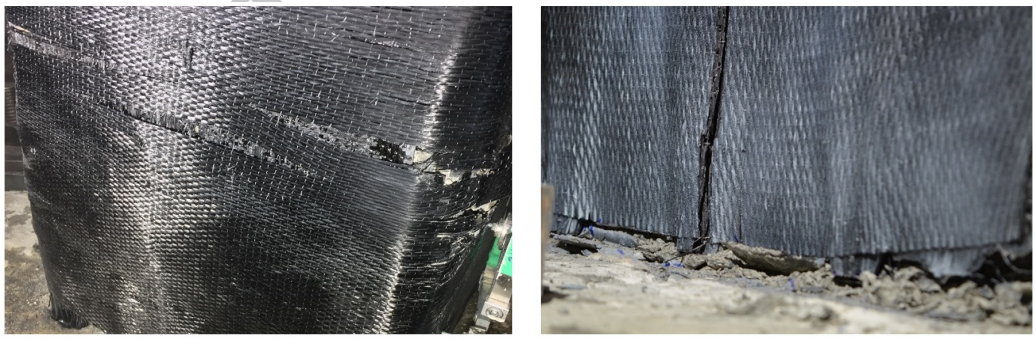

(a) General rupture of the longitudinal FRP sheets – Column 5

(b) Column 2 with all the anchors broken

Fig. 17. Damage in the third stage

ACCEPTED MANUSCRIPT

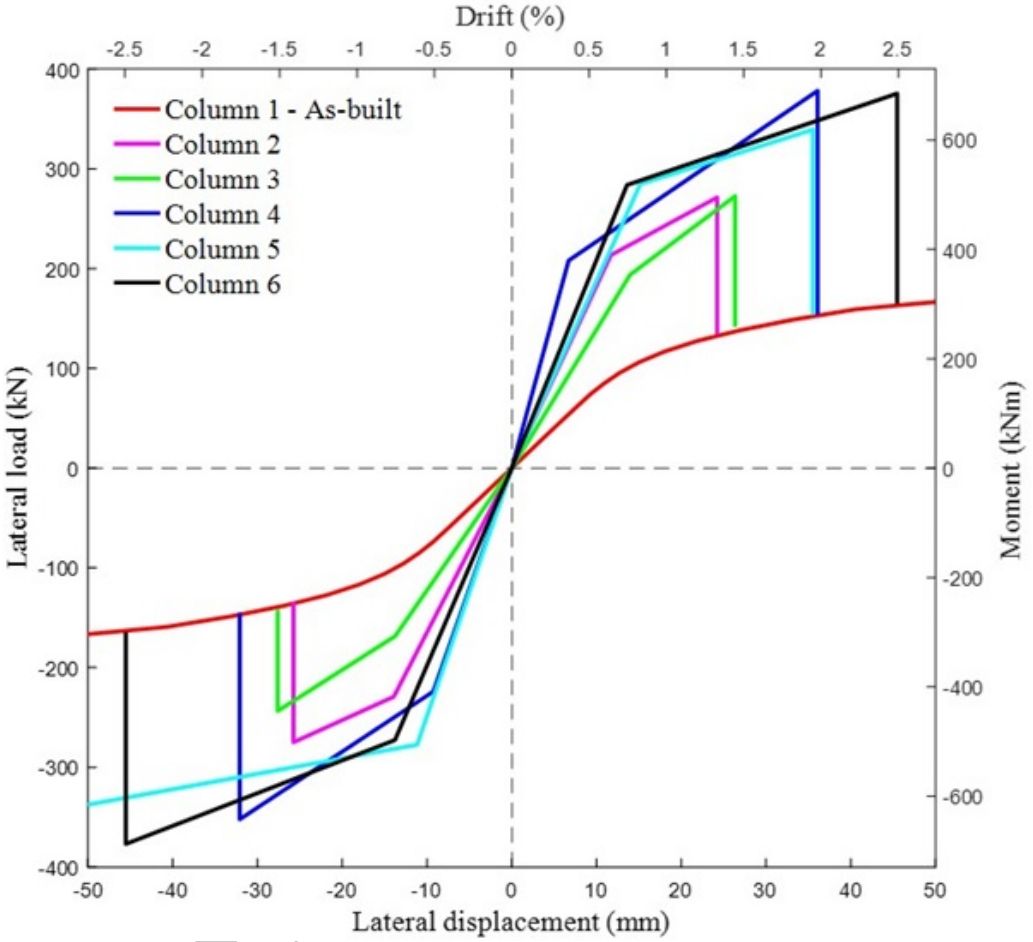

Fig. 18. Summary of column tri-linear behavior

cantly between columns. However, the drift at peak moment differed significantly depending on the amount of FRP material installed on the column. Columns 2 and 3 featured the same longitudinal FRP configuration, and the drift at peak moment was therefore comparable. Column 4 featured more FRP material than did columns 2 and 3 and the drift at peak moment increased accordingly. The behavior of column 5 was highly asymmetrical and might not be comparable to that of the other columns. Finally, column 6 featured the greatest quantity of FRP material of all tested columns, in addition to the bond breaking layer, which contributed to the larger drift of column 6 when compared with all the other columns.

ACCEPTED MANUSCRIPT

3.6. Calculated versus experimental comparison

The experimentally obtained backbone curves are reported in Figure 19, together with the calculated backbone curves obtained using the Response 2000 software. The calculated backbone curves for columns 2 and 3 and for columns 5 and 6 are coincidental. While the moment capacity was correctly forecasted the column stiffness was not accurately calculated, especially during the first stage of response. The stiffness contribution of the FRP materials was different when the FRP sheets were bonded to the concrete surface than when the sheets were debonded. This difference of FRP stiffness was the reason for the disparity observed in the drift ratios between the experimentally obtained and the calculated backbone curves. Future research will need to focus on characterizing the bond behavior of the FRP so that the column ductility can be obtained and correctly implemented into the design.

The calculated and measured debonding moment and the corresponding drift ratio are reported in Table 6, together with the strengthening and ductility ratios. As explained above, the calculated values were obtained using Response 2000, adopting the debond strains calculated with Section 4.1.2 of CNR DT 200[26]. The experimental values were obtained from the hysteresis loops and from the backbone curves and confirmed during testing via cracking sounds and coin-tapping. The strengthening ratio was defined as the ratio between the debonding moment of the strengthened column and the peak moment of the as-built column. Similarly, the ductility ratio was defined as the ratio between the drift ratio at the debonding moment of the strengthened column and the drift ratio at peak moment of the as-built column.

The asymmetric behavior observed in the hysteresis loops reported in Figure 5 is partially quantified in Table 6. The largest debonding moment asymmetry was 13% in column 3 and the maximum debonding drift asymmetry was observed in column 4 with a 42% difference between the push and pull loading directions. The asymmetric response was much larger for the drift capacity than for the moment capacity, except for column 6 that featured the bond breaking layer. The reduced asymmetric response of column 6 indicates that the bond breaking layer might be a good method to homogenize the cyclic column behavior in addition to controlling the column ductility capacity.

The debonding moment increased according to the design, but the debonding drift ratio was similar among all the columns, with the average of the 10 data points being 0.76% and the coefficient of variation being 13.9%. The debond moment capacity was accurately forecasted, with an average difference between calculated and experimental response of 6.2% and maximum deviation of 19.0%.

ACCEPTED MANUSCRIPT

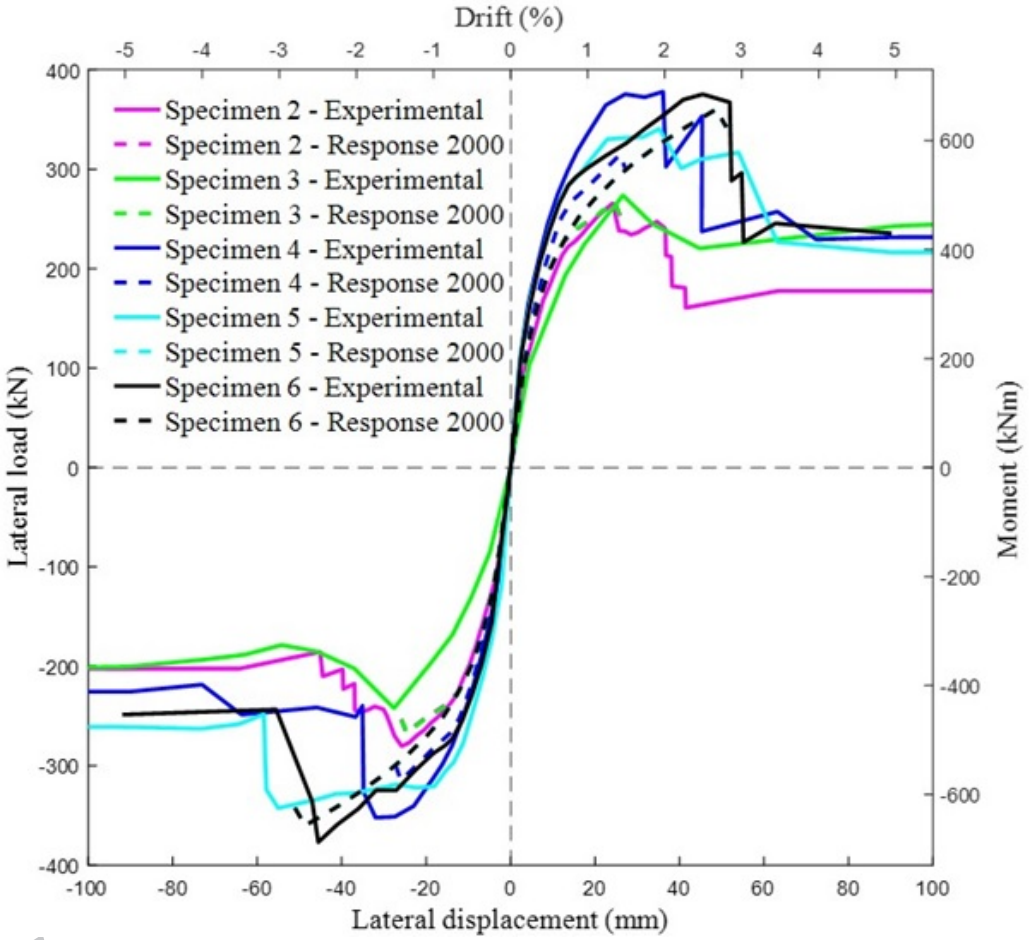

Fig. 19. Experimentally obtained versus calculated backbone curves

ACCEPTED MANUSCRIPT

Table 6. Summary of debonding results

	Debond moment M_d (kNm)			Drift ratio at debond δ_d (%)			Strengthening ratio (M_d/M_i)		Ductility ratio (δ_d/δ_i)	
Column	R2k	Push	Pull	R2k	Push	Pull	Push	Pull	Push	Pull
1	367†	367†	367†	1.15	1.15‡	1.15‡	1	1	1	1
2	381	390	418	0.54	0.64	0.76	1.06	1.14	0.56	0.66
3	380	354	307	0.54	0.76	0.75	0.96	0.84	0.66	0.65
4	425	380	409	0.54	0.72	1.02	1.03	1.11	0.63	0.89
5	499	520	506	0.65	0.83	0.61	1.42	1.38	0.72	0.53
6	499	518	498	0.65	0.74	0.76	1.41	1.36	0.64	0.66

†Obtained with moment curvature analysis using Response 2000,
‡ Point where the ductility of the curve changed to ductile

In contrast, the debonding drift capacity was not accurately forecasted, with an average difference between calculated and experimental response of 32.6% and maximum deviation of 88.9%. The disparity between calculated and experimental drift was probably related to the stiffer behavior of the FRP materials when the FRP sheets are still bonded to the concrete surface.

The peak moment, drift ratio at peak moment, strengthening ratio and ductility ratio are reported in Table 7, similarly to Table 6. As discussed previously, the peak moment and drift ratio at peak moment were calculated using the FRP rupture strain as an input in Response 2000[30]. The experimental values were extracted from the hysteresis loops and verified when a loud explosive noise was heard and the ruptured fibers were visually observed. The peak results were asymmetric, similarly to the debonding results, with the largest asymmetry in peak moment being equal to 12% in column 3 and the maximum asymmetry in drift at peak moment being equal to 65% in column 5. Contrary to the debonding drift ratios, which were comparable between all the columns, the drift ratio at peak load increased from approximately 1.4% in columns 2 and 3 to 1.9% in column 4 and to 2.4% in columns 5 and 6, depending on the amount of FRP material used. Similarly to the debonding moment capacity, the peak moment capacity was also accurately calculated, with an average difference between calculated and experimental of 6.6% and maximum deviation of 20.1%. The drift capacity at peak moment was better forecasted than the drift ratio at debonding, with an average between calculated and experimental response of 13.1% and a maximum deviation of 32%.

ACCEPTED MANUSCRIPT

Table 7. Summary of peak results

	Peak moment M_p (kNm)			Drift ratio at peak δ_p (%)			Strengthening ratio (M_p/M_i)		Ductility ratio (δ_p/δ_i)	
Column	R2k	Push	Pull	R2k	Push	Pull	Push	Pull	Push	Pull
1	367†	367†	367†	1.15	1.15‡	1.15‡	1	1	1	1
2	486	495	502	1.35	1.33	1.41	1.35	1.37	1.16	1.23
3	487	498	444	1.41	1.44	1.51	1.36	1.21	1.25	1.31
4	575	690	643	1.50	1.98	1.76	1.88	1.75	1.75	1.53
5	657	619	630	2.79	1.95	3.01	1.69	1.71	1.70	2.62
6	657	685	688	2.80	2.49	2.30	1.87	1.87	2.17	2.00

†Obtained with moment curvature analysis using Response 2000,
‡ Point where the ductility of the curve changed to ductile

The calculation of drift ratio at peak moment was not as good as the calculation of the peak moment.

4. Conclusions and future work

Six RC columns, five of them flexurally strengthened with FRP sheets and FRP anchors, were designed, built and tested. The design process consisted of sectional analysis using Response 2000, applying the FRP debonding and FRP rupture strain to define the critical moments that characterize the seismic behavior of FRP strengthened RC columns. Two different failure modes were accounted for, being FRP anchor rupture and FRP sheet rupture. The widely used idealized bilinear elasto-perfectly plastic behavior could not capture the behavior of FRP strengthened RC columns because the columns featured two critical moments instead of one, namely the debonding moment and the rupture moment. The column behavior was thoroughly discussed and a tri-linear curve was proposed, based on the two aforementioned moments and on the behavior observed during testing.

Based on the test observations, the tension-compression cycles did not have a significant influence on the capacity of the FRP materials. Similarly, the influence of the FRP transverse confinement on the column response and capacity was negligible. The hysteresis loops and the backbone curves were analyzed and discussed, with special attention was given to the asymmetric behavior of the

ACCEPTED MANUSCRIPT

columns. The implementation of a bond breaking layer at the bottom of the column, next to the column-foundation joint, had a significant influence on the column response. By shifting the line where the FRP-to-concrete debonding started the column ductility capacity increased, while at the same time the debonded section could accommodate the buckling of the sheets in the compression cycles without debonding. This behavior prevented premature debonding in the compression cycles and homogenized the behavior, improving the symmetry of the column response. However, only one column featured the bond breaking layer and further research needs to be undertakeen to corroborate these hypotheses. The calculated and the experimental values were discussed, with accurate results being obtained for moment capacity but inaccurate results being obtained for drift ratios. The disparity in drift ratios was probably due to the different behavior of the FRP materials when the FRP sheets were bonded to the concrete substrate and when the FRP sheets were not bonded to the concrete substrate. This different behavior resulted in different column stiffness that changed the overall behavior. Further work needs to be undertaken to characterize and understand this difference and account for the correct behavior in the design procedure.

5. Acknowledgments

The authors acknowledge the support of the technical staff of the Department of Civil and Environmental Engineering at the University of Auckland. The materials used in this project were supplied by Contech Limited and Sika (NZ) Limited and their contribution to the success of this project is gratefully acknowledged. Funding support provided by the New Zealand Earthquake Commission is highly appreciated. This project was (partially) supported by QuakeCoRE, a New Zealand Tertiary Education Commission-funded Centre.

6. References

[1] J. G. MacGregor, Reinforced concrete: Mechanics and design (Seventh Edition), Pearson Education Inc., New Jersey, U.S.A, 2014.

[2] G. G. Thornton, Cast in concrete : concrete construction in New Zealand 1850-1939, Auckland, New Zealand., Reed, 1996.

[3] ASCE/SEI 41, Seismic Evaluation and Retrofit of Existing Buildings: ASCE Standard ASCE/SEI 41-13, American Society of Civil Engineers (ASCE),

ACCEPTED MANUSCRIPT

Reston, Virginia, U.S.A., 2014. doi:10.1061/9780784412855.
URL http://ascelibrary.org/doi/book/10.1061/9780784412855

[4] M. Rodriguez, R. Park, Repair and Strengthening of Reinforced Concrete Buildings for Seismic Resistance, Earthquake Spectra 7 (3) (1991) 439–459.

[5] L. C. Bank, Composites for Construction: Structural Design with FRP Materials, Hoboken, New Jersey, USA, John Wiley & Sons Inc., 2006.

[6] L. Hollaway, A review of the present and future utilisation of FRP composites in the civil infrastructure with reference to their important in-service properties, Construction and Building Materials 24 (12) (2010) 2419–2445. doi:10.1016/j.conbuildmat.2010.04.062.
URL http://linkinghub.elsevier.com/retrieve/pii/S0950061810001947

[7] Y. Kim, K. Quinn, W. M. Ghannoum, J. O. Jirsa, Strengthening of Reinforced Concrete T-Beams Using Anchored CFRP Materials, ACI Structural Journal 111 (5) (2014) 1027. doi:10.14359/51686805.

[8] S. T. Smith, H. Zhang, Z. Wang, Influence of FRP anchors on the strength and ductility of FRP-strengthened RC slabs, Construction and Building Materials 49 (2013) 998–1012. doi:10.1016/j.conbuildmat.2013.02.006.
URL http://linkinghub.elsevier.com/retrieve/pii/S0950061813001074

[9] S. Qazi, E. Ferrier, L. Michel, P. Hamelin, Seismic retrofitting of RC Shear wall with external bonded CFRP, in: Proceedings of the Tenth International Symposium on Fiber Reinforced Polymer Reinforcement for Concrete Structures (FRPRCS - 10), American Concrete Institute (ACI), Tampa, Florida, USA, 2010.

[10] I. Kim, J. O. Jirsa, O. Bayrak, Use of Carbon Fiber-Reinforced Polymer Anchors to Repair and Strengthen Lap Splices of Reinforced Concrete Columns, ACI Structural Journal 108 (5) (2011) 630.

[11] I. Vrettos, E. Kefala, T. C. Triantafillou, Innovative Flexural Strengthening of Reinforced Concrete Columns Using Carbon-Fiber Anchors, ACI Structural Journal 110 (1) (2013) 63.

ACCEPTED MANUSCRIPT

[12] Y. Matsuzaki, K. Nakano, H. Fukuyama, S. Watanabe, Advanced wrapping system with CF anchor - Shear strengthening of RC columns with spandrel wall, in: Proceedings of the Fifth International Conference on Fiber Reinforced Polymer for Reinforced Concrete Structures (FRPRCS-5), Thomas Telford Ltd., Cambridge, UK, 2001.

[13] R. Kalfat, R. Al-mahaidi, S. T. Smith, Anchorage Devices Used to Improve the Performance of Reinforced Concrete Beams Retrofitted with FRP Composites : State-of-the-Art Review, Journal of Composites for Construction 17 (1) (2013) 14–33. doi:10.1061/(ASCE)CC.1943-5614.0000276.

[14] E. del Rey Castillo, M. C. Griffith, J. M. Ingham, FRP anchors attributes, University of Auckland, 10.17608/k6.auckland.5188456, 2017.

[15] S. J. Kim, S. T. Smith, Pullout Strength Models for FRP Anchors in Uncracked Concrete, Journal of Composites for Construction 14 (4) (2010) 406–414. doi:10.1061/(ASCE)CC.1943-5614.0000097.

[16] R. Kanitkar, S. T. Smith, C. Lewis, An Experimental Investigation on the splay portion of embedded FRP tension anchors, in: Proceedings of The 8th International Conference on Fibre-Reinforced Polymer (FRP) Composites in Civil Engineering (CICE 2016), Department of Civil and Environmental Engineering & Research Institute for Sustainable Urban Development, The Hong Kong Polytechnic University, Hong Kong, China, 2016, pp. 413–418.

[17] K. Q. Walsh, K. J. Elwood, J. M. Ingham, Seismic Considerations for the Art Deco Interwar Reinforced-Concrete Buildings of Napier , New Zealand, Natural Hazards Review 16 (4) (2014) 04014035. doi:10.1061/(ASCE)NH.1527-6996.0000169.

[18] NZS 3112-2, Methods of test for concrete, New Zealand Standards (NZS), Wellington, New Zealand, 1986.

[19] SIKA, SikaWrap ® 600 C Product Data Sheet, SIKA (NZ) Ltd., Auckland, New Zealand, 2013.

[20] SIKA, SikaWrap ® FX-50C Product Data Sheet, SIKA (NZ) Ltd., Auckland, New Zealand, 2014.

[21] SIKA, SikaWrap ® FX-50C Technical Service Report, SIKA Services AG, Madrid, Spain, 2014.

ACCEPTED MANUSCRIPT

[22] ACI 440.2R, Guide for the Design and Construction of Externally Bonded FRP Systems for Strengthening Concrete Structures, American Concrete Institute (ACI) Comittee 440, Farming Hills, Michigan, U.S.A, 2017. doi:10.1061/40753(171)159.
URL http://www.afzir.com/sites/default/files/kb/attached/3.pdf

[23] S. Popovics, A numerical approach to the complete stress-strain curve of concrete, Cement and Concrete Research 3 (5) (1973) 583–599. doi:10.1016/0008-8846(73)90096-3.

[24] F. J. Vecchio, M. P. Collins, The Modified Compression-Field Theory for Reinforced Concrete Elements Subjected to Shear, ACI Journal Proceedings 83 (2) (1986) 219–231. doi:10.14359/10416.
URL http://www.concrete.org/Publications/ACIMaterialsJournal/ACIJournalSearch.aspx?m=details&ID=10416

[25] E. C. Bentz, Sectional analysis of reinforced concrete members, Doctor of Philosophy Thesis at The University of Toronto, Department of Civil Engineering, 2000.

[26] CNR-DT 200, Guide for the Design and Construction of Externally Bonded FRP Systems for Strengthening Existing Structures, CNR (Consiglio Nazionale delle Ricerche) - Advisory Committee on Technical Recommendations for Construction, Rome, Italy, 2013.

[27] ACI 374.2R, Guide for Testing Reinforced Concrete Structural Elements under Slowly Applied Simulated Seismic Loads, American Concrete Institute (ACI) Comittee 374, Farming Hills, Michigan, U.S.A, 2013.

[28] D. A. Bournas, T. C. Triantafillou, Flexural Strengthening of Reinforced Concrete Columns with Near-Surface-Mounted FRP or Stainless Steel, ACI Structural Journal 106 (4) (2009) 495–506. doi:10.14359/56615.
URL http://www.concrete.org/Publications/ACIMaterialsJournal/ACIJournalSearch.aspx?m=details&ID=56615

[29] C. Goksu, A. Polat, A. Ilki, Attempt for Seismic Retrofit of Existing Substandard RC Members under Reversed Cyclic Flexural Effects, Journal of Composites for Construction 16 (3) (2012) 286–299.

ACCEPTED MANUSCRIPT

doi:10.1061/(ASCE)CC.1943-5614.0000256.
URL http://www.scopus.com/inward/record.url?eid=2-s2.0-84862161176&partnerID=tZOtx3y1

[30] E. Bentz, M. Collins, Response 2000 (2000).

ACCEPTED MANUSCRIPT